Breaking Rotational Symmetry in a Self-Organizing Map-Model for Orientation Map Development

M. Riesenhuber

Department of Brain and Cognitive Sciences

and

Center for Biological and Computational Learning,

Massachusetts Institute of Technology, E25-221, Cambridge, MA 02139,

USA,

H.-U. Bauer
D. Brockmann
T. Geisel

Max-Planck-Institut für Strömungsforschung,

Postfach 28 53, 37018 Göttingen, Fed. Rep. of Germany

To appear in Neural Computation

Abstract

We analyze the pattern formation behaviour of a high-dimensional Self-Organizing-Map-model for the competitive projection of ON-center-type and OFF-center-type inputs to a common map layer. We mathematically show, and numerically confirm that even isotropic stimuli can drive the development of oriented receptive fields and an orientation map in this model. This result provides an important missing link in the spectrum of pattern formation behaviours observed in SOM-models. Extending the model by including further layers for binocular inputs, we also investigate the combined development of orientation and ocular dominance maps. A parameter region for combined patterns exists; corresponding maps show a preference for perpendicular intersection angles between iso-orientation lines and ocularity domain boundaries, consistent with experimental observations.

1 Introduction

Topographic maps are an ubiquitous pattern of organization in the brain. Among the most intensely investigated such patterns are orientation maps and ocular dominance maps in the visual cortex. Various models have been formulated which generate topographic maps as a consequence of activity driven self-organization processes (see Erwin *et al.*, 1995, Swindale, 1996, for two recent reviews). The simulated maps coincide with observed maps in many aspects. Yet distinctive differences remain, between simulated and observed maps as well as between simulated maps from different modeling frameworks. The better we can relate such differences to specific underlying assumptions, the more differences we can eliminate, and the more experimental observations we can account for within universal modeling frameworks, the more stable our understanding of map self-organization processes will become.

A few years ago, two map formation models have been presented which generate oriented receptive fields from a competition of ON-center and OFF-center cell responses in the LGN (Miller, 1992, 1994, Miyashita and Tanaka, 1992). These models elegantly explain how orientation-selective simple cell responses could be due to a self-organization process which is driven by non-patterned input activity and could take place even before birth. Without discussing any of the details of these models, we just note that their inputs are non-oriented, yet the resulting patterns break this symmetry.

A third, rather widely applied framework for map development is Kohonen's

Self-Organizing Map algorithm (SOM). SOM-based models have sucessfully accounted for various aspects of visual (Obermayer *et al.*, 1990, 1992, Goodhill, 1993, Wolf *et al.*, 1994, 1996, Bauer *et al.*, 1997), auditory (Martinetz *et al.*, 1988) and somatosensory (Ritter and Schulten, 1986, Andres *et al.*, 1994) map formation. Yet, in simulations of SOM-based models for ON-center and OFF-center-cell competition, a break of rotational symmetry has not been observed so far, despite a long-lasting search in several groups. This negative outcome could be the consequence of a suboptimal selection of parameters, or it could be the fingerprint of a fundamental difference between SOM-based models and the above-mentioned models by Miyashita and Tanaka, and by Miller. Clarification of this issue is an interesting problem not only with regard to explanations of orientation map development, but in particular with regard to theoretical consistency between modeling frameworks.

In this letter we finally report that also SOMs can break rotational symmetry, albeit in a quite small regime of parameters. Using a recently described analysis technique (Riesenhuber *et al.*, 1996, Bauer *et al.*, 1997), we first mathematically analyze the pattern formation behaviour of the corresponding SOM-model. After a short introduction to the SOM in the second section, analytical results are described in the third section. Guided by the mathematical analysis, we also performed simulations of the model, the results of which are given in the fourth section. Finally, in the fifth section, we investigate the development of combined orientation and ocular dominance maps.

2 "High-dimensional" SOM-model for the development of orientation maps from non-oriented stimuli

Neurons in a Self-Organizing Map (SOM) are characterized by positions $\mathbf{r}$ in a map lattice $\mathcal{A}$, and receptive fields $\mathbf{w_r}$ in a map input space $\mathcal{V}$. The input space is assumed to consist of one (or several) layer(s) of input channels. The typically large number of input channels give rise to the notion of a high-dimensional SOM, as opposed to a feature map description. As a consequence, stimuli $\mathbf{v} \in \mathcal{V}$ are activity distributions, and receptive fields $\mathbf{w_r}$ are synaptic weight distributions. A stimulus $\mathbf{v}$ is mapped onto that neuron $\mathbf{s} \in \mathcal{A}$, whose receptive field $\mathbf{w_s}$ matches $\mathbf{v}$ best,

$$\mathbf{s} \;=\; \arg\max_{\mathbf{r}\in\mathcal{A}}\{\mathbf{w_r}\cdot\mathbf{v}\}. \tag{1}$$

Presenting a random sequence of stimuli and performing adaptation steps,

$$\Delta\mathbf{w_r} \;=\; \epsilon h(\mathbf{r}-\mathbf{s})\,(\mathbf{v}-\mathbf{w_r})\,, \tag{2}$$

the internal shape of individual receptive fields as well as the map layout self-organize simultaneously. The neighborhood function $h(\mathbf{r}-\mathbf{s})$,

$$h(\mathbf{r}-\mathbf{s}) \;=\; \exp\left(-\frac{\|\mathbf{r}-\mathbf{s}\|^2}{2\sigma^2}\right), \tag{3}$$

ensures that neighboring neurons align their receptive fields, *i.e.,* it imposes topography on the map. A comprehensive treatment of many theoretical and application-related aspects of SOMs can be found in Ritter *et al.* (1992) and Kohonen (1995).

Within this general framework, we now consider a projection geometry analogous to that proposed by Miller (1992, 1994) and Miyashita and Tanaka (1992). Cells in ON-center and OFF-center input layers project to the map layer. As would result from a filtering of point-like retinal stimuli by thalamic ON-center and OFF-center cells, we assume our stimuli to consist of an activity peak in one layer, plus an activity annulus in the other layer.

Mathematically, stimuli are represented as difference-of-Gaussians (DOG) (stimulus center position: $\mathbf{x_0}$, widths of the two Gaussians: $\sigma_{1,2}$, relative amplitude of the Gaussians: k),

$$\mathbf{a}(\mathbf{x};\mathbf{x}_0) = \exp\left(\frac{-\|\mathbf{x}-\mathbf{x}_0\|^2}{2\sigma_1^2}\right) - k\exp\left(\frac{-\|\mathbf{x}-\mathbf{x}_0\|^2}{2\sigma_2^2}\right). \tag{4}$$

Furthermore, $\mathbf{a}_\bullet(\mathbf{x};\mathbf{x}_0) = [\mathbf{a}(\mathbf{x};\mathbf{x}_0)]_+$ denotes the activity distribution of the central peak of the DOG, and $\mathbf{a}_\circ(\mathbf{x};\mathbf{x}_0) = [-\mathbf{a}(\mathbf{x};\mathbf{x}_0)]_+$ the annulus-shaped activity distribution corresponding to the negative part of the DOG ($[\cdot]_+$ is the rectification operator). Naturally, ON-type and OFF-type stimuli are represented as two-component vectors,

$$\mathbf{v}_{\mathrm{ON}} = (\mathbf{a}_\bullet, \mathbf{a}_\circ), \quad \mathbf{v}_{\mathrm{OFF}} = (\mathbf{a}_\circ, \mathbf{a}_\bullet), \tag{5}$$

each component describing the (non-negative) activity distribution in one of the input layers. In the simulations, the center positions $\mathbf{x_0}$ and polarity (*i.e.*, whether the stimulus is $\mathbf{v}_{\mathrm{ON}}$ or $\mathbf{v}_{\mathrm{OFF}}$) are chosen at random.

3 Mathematical results on the formation of oriented receptive fields

Recently, Riesenhuber *et al.* (1996) and Bauer *et al.* (1997) described a new technique to calculate conditions on stimulus and map parameters for the emergence of non-trivial patterns in high-dimensional SOMs. This technique makes use of a distortion measure $E_{\mathbf{v}}$ which is evaluated for different potentially stable states of the map and which is assumed to be minimized by the SOM-algorithm. A crucial feature of the method is the way in which "potentially stable states" of a SOM are formalized. While an explicit characterization of such states in terms of the weight vectors $\mathbf{w}_{\mathbf{r}}$ seems impossible without actually simulating the SOM, the states can also be characterized by the way they distribute stimuli among map neurons (the tesselation). This is specific to the SOM, where the winner-take-all mapping rule (1) assigns a particular map neuron to each stimulus.

Denoting by $\Omega_{\mathbf{r}}$ all stimuli which are mapped to neuron $\mathbf{r}$ (the *Voronoi cell* of $\mathbf{r}$), we define a distortion measure

$$E_{\mathbf{v}} = \sum_{\mathbf{r},\mathbf{r}'} h(\mathbf{r}-\mathbf{r}')\, w(\mathbf{r},\mathbf{r}'), \tag{6}$$

$$w(\mathbf{r},\mathbf{r}') = \sum_{\mathbf{v}\in\Omega_{\mathbf{r}}} \sum_{\mathbf{v}'\in\Omega_{\mathbf{r}'}} (\mathbf{v}-\mathbf{v}')^2. \tag{7}$$

Each term in $E_{\mathbf{v}}$ consists of the mean squared difference $w(\mathbf{r},\mathbf{r}')$ between stimuli within the same, or between neighboring, Voronoi cells, weighted by the neighborhood function $h(\mathbf{r}-\mathbf{r}')$. The definition of $E_{\mathbf{v}}$ is motivated by the analogy of SOMs to vector quantizers (see Riesenhuber *et al.* (1996)). Qual-

itatively different states of a map yield different values of $E_{\mathbf{v}}$ because they correspond to different tesselations $\{\Omega_{\mathbf{r}}\}$. What are the typical tesselations in the present context?

To simplify the analysis we assume an equal number of ON-center input channels, OFF-center input channels, and map neurons, with a basically retinotopic projection. We further assume that the stimulus center positions $\mathbf{x}_0$ are constrained to the positions of the input channels, resulting in twice as many stimuli as map neurons. Three qualitatively different possible map states can be distinguished:

- System $\mathcal{B}$: Each neuron responds to both an ON- and an OFF-stimulus, each located at the same retinal position. This tesselation yields neurons with orientation insensitive receptive fields.

- System $\mathcal{S}$: As in system $\mathcal{B}$, each neuron responds to stimuli of both polarities, but now displaced one step along one retinal coordinate. The displacement breaks isotropy. It causes the receptive fields to exhibit internal ON-center and OFF-center structure, with orientation specificity.

- System $\mathcal{O}$: Here each neuron responds to two retinally neighboring stimuli of identical polarity. Although this tesselation induces an orientation specificity, it also breaks the symmetry between ON-center and OFF-center inputs to each neuron. Neurons segregate into ON-center and OFF-center dominated populations, analogous to an ocular dominance map. While this state is an imaginable (and numerically

observed, see below) state of SOMs, we do not consider this state as biologically interesting.

To evaluate $w(\mathbf{r},\mathbf{r}')$ and $E_{\mathbf{v}}$ for these tesselations, we need to consider the difference δ^s between two stimuli of same polarity, separated by a distance of $\Delta\mathbf{x}_0 = \mathbf{x}_0 - \mathbf{x}_0'$,

$$\delta^s(\Delta\mathbf{x}_0) = \sum_{\mathbf{x}} \left(\mathbf{a}_\bullet(\mathbf{x},\mathbf{x}_0) - \mathbf{a}_\bullet(\mathbf{x},\mathbf{x}_0')\right)^2 + \left(\mathbf{a}_\circ(\mathbf{x},\mathbf{x}_0) - \mathbf{a}_\circ(\mathbf{x},\mathbf{x}_0')\right)^2, \quad (8)$$

and the difference δ^a between two oppositely polarized stimuli,

$$\delta^a(\Delta\mathbf{x}_0) = \sum_{\mathbf{x}} \left(\mathbf{a}_\bullet(\mathbf{x},\mathbf{x}_0) - \mathbf{a}_\circ(\mathbf{x},\mathbf{x}_0')\right)^2 + \left(\mathbf{a}_\circ(\mathbf{x},\mathbf{x}_0) - \mathbf{a}_\bullet(\mathbf{x},\mathbf{x}_0')\right)^2. \quad (9)$$

Using these distances, and exploiting the isotropy with respect to one retinal coordinate, we obtain for the interaction terms w (Eq. 7):

$$w^{\mathcal{B}}(\Delta r) = \delta^s(\Delta r) + \delta^a(\Delta r), \quad (10)$$

$$w^{\mathcal{S}}(\Delta r) = \delta^s(\Delta r) + \frac{1}{2}\left\{\delta^a(\Delta r - 1) + \delta^a(\Delta r + 1)\right\}, \quad (11)$$

$$w^{\mathcal{O}}(\Delta r) = \sum_{i=s,a} \frac{1}{2}\,\delta^i(\Delta r) + \frac{1}{4}\left\{\delta^i(\Delta r + 1) + \delta^i(\Delta r - 1)\right\}. \quad (12)$$

Inserting (10-12) into Eq. (6), and performing a numerical summation, we obtain the distortion measures $E^{\mathcal{B}}_{\mathbf{v}}$, $E^{\mathcal{S}}_{\mathbf{v}}$ and $E^{\mathcal{O}}_{\mathbf{v}}$. This analysis predicts that, depending on the stimulus parameters $\sigma_{1,2}, k$, and the map neighborhood parameter σ, different final states of the map will be attained. Fig. 1a shows a state diagram in the σ, k-plane, at widths $\sigma_1 = 1,\ \sigma_2 = 2$. At large values of the annulus amplitude k, receptive fields segregate into "monopolar" ON- and OFF-receptive fields. Large values of the neighborhood width σ prohibit internal structure of the receptive fields to occur. Only in a rather small regime of σ, k-values, the biologically interesting map state $\mathcal{S}$ is attained.

4 Numerical results

To corroborate the mathematical analysis above and to actually obtain orientation maps we also investigated the model numerically. In a first series we ran simulations with 16×16 neuron maps, at various values of σ and k. Classifying the resulting receptive fields with regard to the states $\mathcal{B}, \mathcal{S}, \mathcal{O}$, we obtained the state diagram depicted in Fig. 1b which corresponds quite well to the mathematically obtained diagram.

To obtain receptive fields with a fine spatial resolution, we also simulated maps with 48×48-channel input layers, projecting to a 24×24-neuron map layer. Fig. 2 shows exemplary receptive fields of neurons in a 4×8 segment of the map. The receptive fields show a multi-lobed structure and are clearly oriented. The variation of orientation over the whole map is shown in an angle map in Fig. 3, where the preferred orientation of each cell is given by a circular color code. As in orientation maps obtained by optical imaging methods in the cat (Bonhoeffer *et al.*, 1991) or monkey (Blasdel and Salama, 1986), we find a patchy arrangement of different preferred orientations and also pinwheel-like singularities.

In addition to the map of prefered orientation angles of the receptive fields, we also calculated the phases of the receptive field, *i.e.,* the shift angles which would occur in a Gabor function fit to the receptive field profile (see caption of Fig. 3). It has been hypothesized that the phase angle is also arranged in a topographic fashion in the primary visual cortex, with a topology of the combined orientation and phase stimulus space equivalent to that of a Klein

bottle (Tanaka, 1995). In our simulated maps we find the phase angle to vary indeed in a smooth way in many areas of the map (see arrows in Fig. 3). Phase and orientation values are not correlated. 2π-singularities can be found in the phase, at locations other than the locations of orientation singularities. So all the topological properties we could identify in our map are consistent with Tanaka's suggestion of the Klein bottle topology.

5 Development of combined orientation and ocular dominance maps

Finally, we complemented the two ON-center and OFF-center input cell layers for one eye by two further ON-center and OFF-center cell layers for the other eye. The repertoire of possible patterns in this extended model should go beyond merely oriented receptive fields in an orientation map, it should also include monocular receptive fields and ocular dominance maps, and combinations of the two types of patterns.

Stimuli in the extended model consist of activity distributions in all four input layers. While the difference in shape of the activity distributions between ON-center and OFF-center layers is the same as before, the partial stimuli are assumed to be of identical shape in the corresponding layers for either eye, but attenuated by a factor of c, $0 \leq c \leq 1$, in one of the eyes (analogous to the assumptions underlying a recently analyzed SOM-based model for ocular dominance formation (Bauer *et al.*, 1997, see also Goodhill, 1993). This yields, apart from the random variations of the stimulus center, four

different types of stimuli:

$$\mathbf{v}_{\mathrm{L,ON}} = \begin{pmatrix} \mathbf{a}_\bullet \\ \mathbf{a}_\circ \\ c \cdot \mathbf{a}_\bullet \\ c \cdot \mathbf{a}_\circ \end{pmatrix}, \qquad \mathbf{v}_{\mathrm{L,OFF}} = \begin{pmatrix} \mathbf{a}_\circ \\ \mathbf{a}_\bullet \\ c \cdot \mathbf{a}_\circ \\ c \cdot \mathbf{a}_\bullet \end{pmatrix},$$

$$\mathbf{v}_{\mathrm{R,ON}} = \begin{pmatrix} c \cdot \mathbf{a}_\bullet \\ c \cdot \mathbf{a}_\circ \\ \mathbf{a}_\bullet \\ \mathbf{a}_\circ \end{pmatrix}, \qquad \mathbf{v}_{\mathrm{R,OFF}} = \begin{pmatrix} c \cdot \mathbf{a}_\circ \\ c \cdot \mathbf{a}_\bullet \\ \mathbf{a}_\circ \\ \mathbf{a}_\bullet \end{pmatrix}. \tag{13}$$

The analysis technique introduced in section 3 can be applied to this more complicated case as well, considering the different tesselation possibilities for four stimuli per neuron. To save space, we omit the details of the rather lengthy calculations, and proceed to a description of the results. Since we have five parameters in the model now (σ_1, σ_2, k for the DOG, c for the between-eye correlations, and σ as a map control parameter), the full state diagram cannot be depicted. Instead, we show in Fig. 4a a section in the k-c-plane. Regions with orientation only, and with ocular dominance only are found. Most importantly, there is a region with a combination of both orientation and ocular dominance at small values of k and c.

In computer simulations we found maps with monocular receptive fields, oriented receptive fields, or combined monocular, oriented receptive fields, each in the parameter regimes predicted by the analysis (see Fig. 4b). Fig. 5 shows one combined map in a plot that displays the boundaries of the isoocularity domains superimposed on the color-coded orientation map.

Determining the transition lines between isoocularity regions in the simulated map, and computing the intersection angles with the isoorientation lines at

these locations, we compiled an angle histogram (Fig. 6). Isoorientation lines intersect the boundaries between isoocularity regions preferably at larger angles, consistent with experimental observations by Bartfeld *et al.* (1992) and Obermayer and Blasdel (1993).

6 Discussion

In this letter we showed mathematically and numerically how in a high-dimensional SOM-model for the competitive projection of ON-center and OFF-center inputs to a common map layer a rotation symmetry of stimuli can be broken to yield oriented receptive fields. This pattern formation behaviour can be described only in a high-dimensional map formation framework, which allows to also consider the internal structure of receptive fields. In low-dimensional feature map models, where each map dimension corresponds to a particular stimulus and receptive field parameter, a non-trivial structure along a particular dimension cannot be obtained, if the stimuli have no extension along this dimension (as is the case for round stimuli with respect to an orientation dimension). A break of isotropy has already been observed in other frameworks for map development models (Miyashita *et al.*, 1992, Miller, 1992, 1994). The results we describe here for the SOM-framework close a somewhat puzzling gap in the qualitative behaviour of these different frameworks, reducing the relative importance of the specific mathematical formalisations, and increasing the importance of common mechanisms.

Our results are based not only on numerical simulations, but also on a math-

ematical analysis. The coincidence of the mathematically derived parameter regimes for particular map structures and the numerical observation of these structures underlines the value of our energy formalism to analyze pattern formation in high-dimensional SOM-models and to guide simulations of these models. For the case of combined ocular dominance and orientation maps, the analysis turned out to involve a substantially larger number of map patterns which need to be considered. The increase in effort necessary for the two-variable case suggests that this kind of analysis is unfeasible for maps with three underlying symmetries. For the combined maps we identified a parameter regime in which ocular dominance and orientation structure stably coexist. In the correlation-based framework, combined maps were numerically found to exist (Erwin and Miller, 1995), but the mathematical underpinnings were judged controversely (Piepenbrock *et al.*, 1996, 1997).

Acknowledgements

Interesting discussions with Ken Miller and Fred Wolf are gratefully acknowledged. This work has been supported by the Deutsche Forschungsgemeinschaft through Sonderforschungsbereich 185 Nichtlineare Dynamik, TP E6.

References

Andres, M. Schlüter, O. Spengler, F. Dinse, H. R. 1994. A model of fast and reversible representational plasticity using Kohonen mapping, in: Proc. ICANN94, Sorrento, Eds. M. Marinao, P. G. Morasso, Springer, Berlin, 306-309.

Bartfeld, E., Grinvald A. 1992. Relationship between orientation preference pinwheels, cytochrome oxidase blobs and ocular-dominance columns in primate striate cortex. *Proc. Nat. Acad. Sci. USA* **89**, 11905-11909.

Bauer, H.-U. Brockmann, D. Geisel, T. 1997. Analysis of ocular dominance pattern formation in a high-dimensional self-organizing-map-model. *Network* **8**, 17-33.

Blasdel, G. G., Salama, G. 1986. Voltage-sensitive dyes reveal a modular organization in monkey striate cortex. *Nature* **321**, 579-585.

Bonhoeffer, T., Grinvald, A. 1991. Iso-orientation domains in cat visual cortex are arranged in pinwheel-like patterns. *Nature* **353**, 429-430.

Erwin, E., Obermayer, K., Schulten, K. 1995. Models of orientation and ocular dominance columns in the visual cortex: A critical comparison. *Neur. Comp.* **7**, 425-468.

Erwin, E. Miller, K. D. 1996. Modeling joint development of ocular dominance and orientation maps in primary visual cortex. *Computational Neuroscience (Proc. CNS 1995)*, Ed. J. Bower, 179-184.

Goodhill, G. J. 1993. Topography and ocular dominance: a model exploring positive correlations. *Biol. Cyb.* **69** 109-118.

Kohonen, T., 1995. The Self-Organizing Map, Springer.

Martinetz, T., Ritter, H., Schulten, K. 1988. Kohonen's self-organizing map for modeling the formation of the auditory cortex of a bat. In: SGAICO-

Proceedings "Connectionism in Perspective", 403-412.

Miller, K. D. 1992. Development of orientation columns via competition between ON- and OFF-center inputs. *NeuroRep.* **3**, 73-79.

Miller, K. D. 1994. A model for the development of simple-cell receptive fields and the ordered arrangement of orientation columns through activity dependent competition between On- and Off-center inputs, *J. Neurosci.* **14**, 409-441.

Miyashita, M. Tanaka, S. 1992. A mathematical model for the self-organization of orientation columns in visual cortex. *NeuroRep.* **3**, 69-72.

Obermayer K., Ritter, H., Schulten, K., 1990. A principle for the formation of the spatial structure of cortical feature maps, *Proc. Nat. Acad. Sci. USA* **87**, 8345-8349.

Obermayer, K., Blasdel, G. G., Schulten, K. 1992. Statistical-mechanical analysis of self-organization and pattern formation during the development of visual maps. *Phys. Rev. A* **45**, 7568-7569.

Obermayer, K., and Blasdel, G. G., 1993. Geometry of orientation and ocular dominance columns in monkey striate cortex, *J. Neurosci.* **13** 4114–4129.

Piepenbrock, C., Ritter, H., Obermayer, K. 1996. Linear correlation-based learning models require a two-stage process for the development of orientation and ocular dominance, *Neur. Proc. Lett.* **3**, 1-7.

Piepenbrock, C., Ritter, H., Obermayer, K. 1997. The joint development

of orientation and ocular dominance: role of constraints, *Neur. Comp.* **9**, 959-970.

Riesenhuber, M., Bauer, H.-U., Geisel, T. 1996. Analyzing phase transitions in high-dimensional self-organizing maps, *Biol. Cyb.* **75**, 397-407.

Ritter, H., Schulten, K. (1986). On the stationary state of Kohonen's self-organizing sensory mapping. *Biol. Cyb.* **54**, 99-106.

Ritter, H., Martinetz, T., Schulten, K., 1992. Neural computation and self-organizing maps. Addison Wesley, Reading, Mass.

Swindale, N. V. 1996. The development of topography in the visual cortex: a review of models, *Network* **7**, 161-247.

Tanaka, S. 1995. Topological analysis of point singularities in stimulus preference maps of the primate visual cortex. *Proc. R. Soc. Lond. B*, **261**, 81-88.

Wolf, F., Bauer, H.-U., Geisel, T. 1994. Formation of field discontinuities and islands in visual cortical maps. *Biol. Cyb.* **70**, 525-531.

Wolf, F., Bauer, H.-U.,, Pawelzik, K., Geisel, T. 1996. Organization of the visual cortex. *Nature* **382**, 306-307.

Figure Captions

Fig. 1: Analytical (**a**) and numerical (**b**) phase diagrams for the SOM-orientation map model. The parameters σ and k denote the neighborhood width of the SOM-algorithm, and the annulus amplitude of the stimuli, respectively. The + symbol denotes the non-oriented state $\mathcal{B}$, $\star$ denotes the oriented state $\mathcal{S}$, and $\triangle$ the (non-biological) state $\mathcal{O}$. In both diagrams further parameters were $\sigma_1 = 1$, $\sigma_2 = 2$, in the numerical maps we applied 10^5 learning steps, learning step size was decreased from $\epsilon_{init} = 0.2$ to $\epsilon_{final} = 0.01$, the neighborhood width σ was kept constant during the simulation.

Fig. 2: Sample receptive fields of a SOM orientation map (4×8 segment of a 24×24-neuron SOM, with two 48×48 input layers, periodic boundary conditions). Further parameters of the simulation were: $\sigma_1 = 3.4$, $\sigma_2 = 6.8$, $k = 0.3$, width of SOM neighborhood function $\sigma = 0.85$, 3×10^5 learning steps, $\epsilon = 0.1 \rightarrow 0.01$. For each neuron, the difference between ON-center and OFF-center cell layer connection strengths is shown as a gray value image. The gray background means no connection strength, black and white regions indicate preferred connections to the ON- or OFF-center layers.

Fig. 3: The complete map described in the caption of Fig. 2, but now depicted as an angle map using a circular color code for the preferred orientation angles of each cell. Superimposed on the color-coded orientation map, we show (as arrows) the phase angle of the receptive fields. The phase angle is calculated by rotating each receptive field by the inverse of its preferred orientation (so that the lobes of an ideal bilobed receptive would fall on different sides of the horizontal meridian after rotation) and then determining the phase shift as compared to a dampened sine wave (*i.e.*, a Gabor filter) of the receptive field profile. A rightward arrow designates a phase of zero degrees,

i.e., the receptive field is bilobed with the positive lobe being in the upper hemisphere after rotation. An upward arrow represents a phase angle of 90^o, *i.e.*, a trilobed receptive field with the negative lobe in the middle. Crosses and circles shows examplary locations of orientation and phase singularities, respetively.

Fig. 4: Phase diagram for combined orientation and ocular dominance maps, as a function of ON-OFF-stimulus parameter k and between-eye-correlation parameter c, at $\sigma_1 = 0.84$, $\sigma_2 = 1.68$, $\sigma = 1.0$. "$\circ$": states with unoriented receptive fields. "+": oriented, binocular receptive fields. "$\star$": monocular receptive fields with type $\mathcal{O}$ ON-center OFF-center cell segregation. "Λ": monocular, oriented receptive fields. **a** shows the analytically obtained diagram, **b** the the diagram resulting from classification of the receptive fields of simulated maps.

Fig. 5: Combined ocular dominance and orientation map, with stimulus parameters as described in the caption of Fig. 4. The orientation angle map is given in color code (as in Fig. 3), the isoocularity domain boundaries are superimposed as black lines. Further parameters are: 24×24-neuron SOM, 34×34-channel input layers, $\sigma = 0.71$, 3×10^5 learning steps, $\epsilon = 0.1 \rightarrow 0.01$, periodic boundary conditions.

Fig. 6: Histogram of angle of intersection of isoorientation lines, and isoocularity domain boundaries, computed for all cells along isoocularity domain boundaries of the map shown in Fig. 5.

Fig. 1:

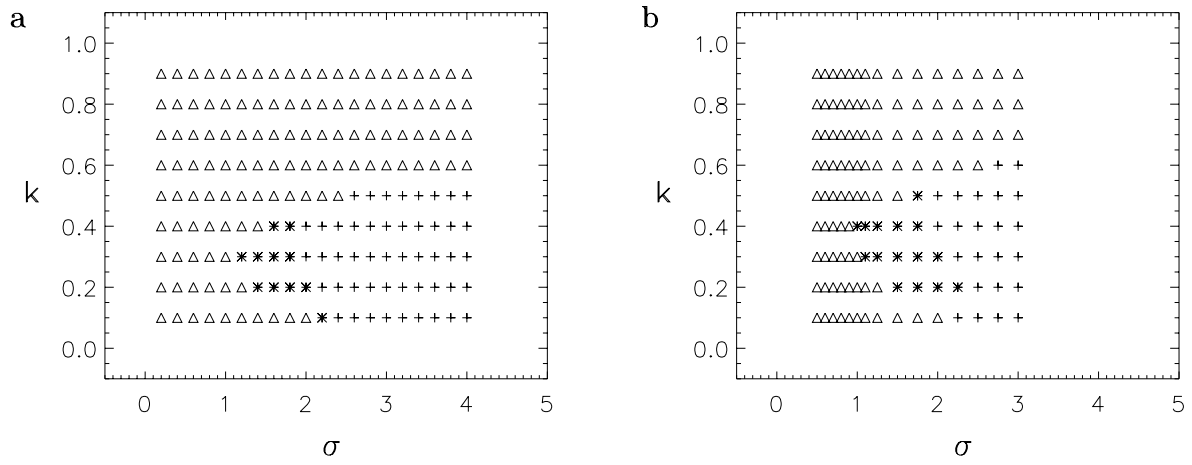

Fig. 2:

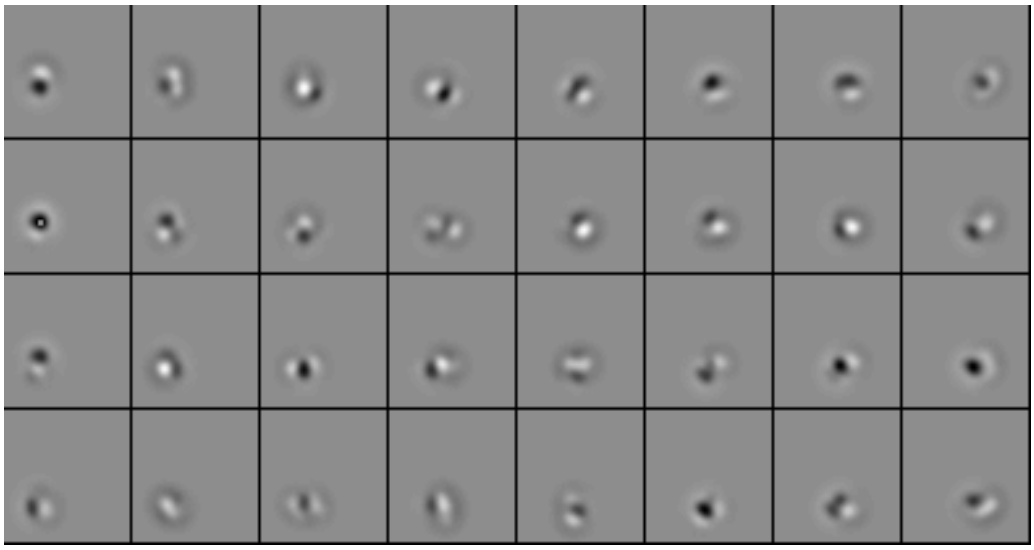

Fig. 3:

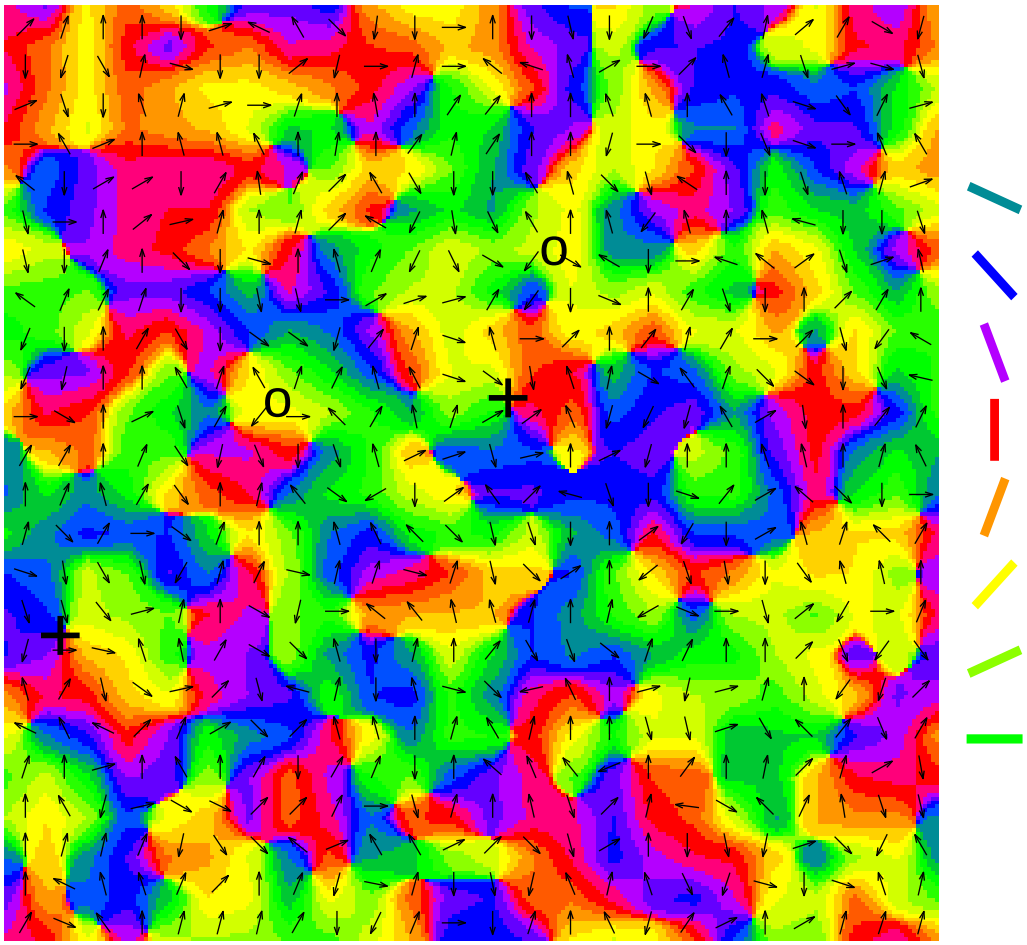

Fig. 4:

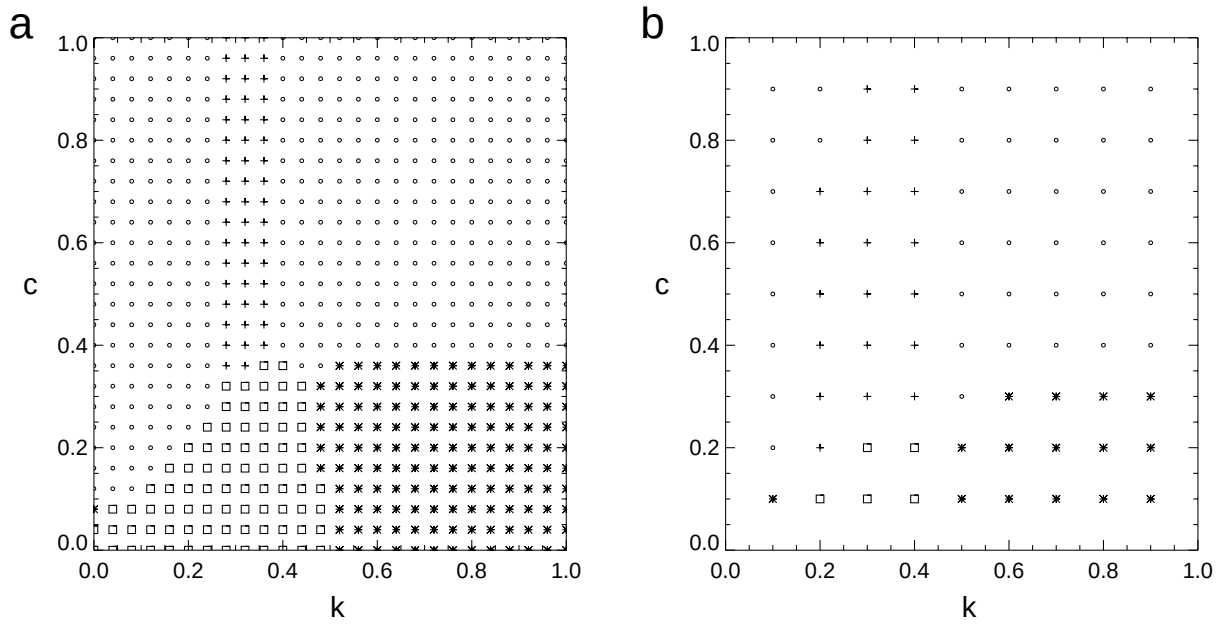

Fig. 5:

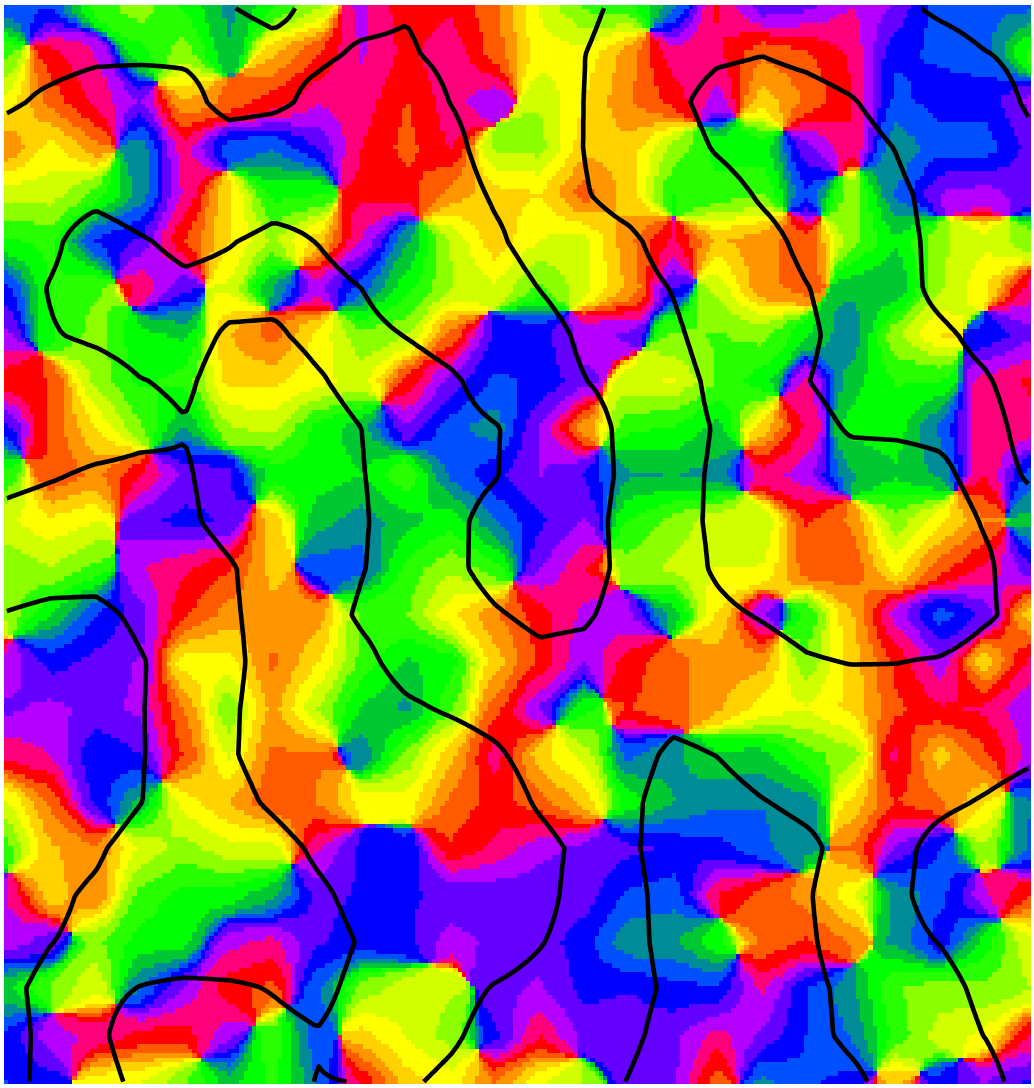

Fig. 6:

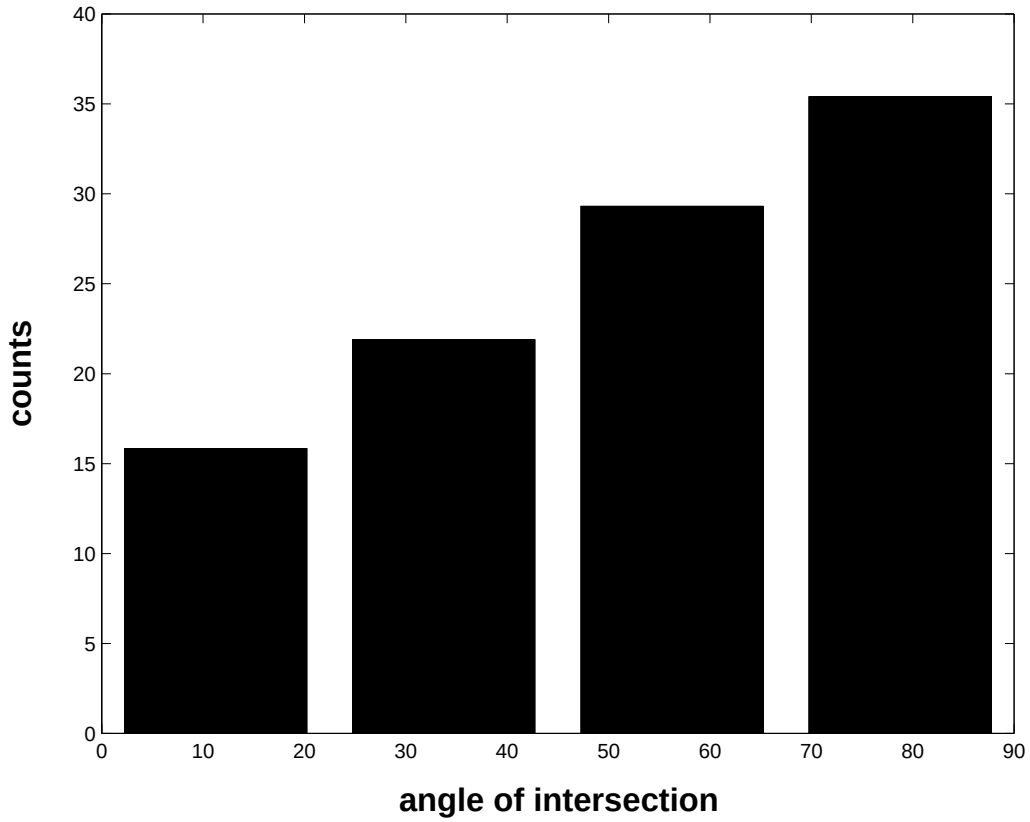
counts
angle of intersection
0
5
10
15
20
25
30
35
40
0
10
20
30
40
50
60
70
80
90